Multi–temperature fluid–dynamic model equations from kinetic theory in a reactive gas: the steady shock problem

M. Bisi[†], G. Martalò[♯], G. Spiga[†]

[†] Dip. di Matematica e Informatica, Università di Parma,

Parco Area delle Scienze 53/A, I-43124 Parma, Italy,

E-mail: marzia.bisi@unipr.it, giampiero.spiga@unipr.it *(corresponding author)*

[♯] Dip. di Matematica, Università di Milano, Via C. Saldini 50, I-20133, Milano

E-mail: giorgio.martalo@unimi.it

Abstract

Starting from a simple kinetic model for chemical reaction, multi–temperature reactive Euler equations are derived for physical regimes in which evolution is driven by elastic collisions within the same species and mechanical relaxation is faster than the thermal one. The achieved hydrodynamic equations, where all inhomogeneous exchange rates take analytical closed form for simple collision models, are then used for the analysis of the steady shock problem. Results indicate that smooth shock profiles occurring for slightly supersonic flows bifurcate to weak solutions (jump discontinuity followed by a smooth tail) for increasing Mach number.

Keywords: Kinetic theory, Reactive gas mixtures, Multi–temperature models, Steady shock waves.
Classification codes: 82C40, 76P05, 80A32, 76V05.

1 Introduction

Modelling and analysis of gas mixtures have been and are being very stimulating and challenging problems of practical significance, especially if one wants to account for non–conservative effects like chemical reactions. The problem can be handled in the frame of the continuum theory of fluids, but of course a consistent derivation of the relevant fluid–dynamic equations from a kinetic approach is highly desirable [1, 2, 3]. Typically, relaxation to thermodynamical equilibrium might occur on different scales: for instance, when masses are disparate, a first Maxwellization step within each species is followed by a slower equilibration of velocities and temperatures [4]. Indeed, when vibrational and chemical relaxations proceed at the slower gas–dynamic time scale, a one–temperature gas flow description is not valid any more [5]. On the other hand, a multi–temperature approach is needed in several problems of aerothermodynamics [6] or in plasmas at high

temperatures [7]. The subject has been quite intensively investigated by methods from extended thermodynamics [8, 9, 10]. Work on multi–temperature equations as hydrodynamic limit of kinetic equations is in progress, starting from suitable models for chemical reactions and state transitions [11, 12], and introducing different scales for different microscopic interactions, according to the process(es) considered as dominant. In particular it was shown in [13] that consideration, in an Euler description, of one velocity and one vibrational temperature for each species and of a single translational temperature for the whole gas, may be induced by dominance of purely elastic scattering in the presence of resonance effects induced by degeneracy of internal energy levels. Multi–temperature and multi–velocity Euler equations were obtained also in [14], for a non reactive polyatomic mixture without degeneracy, when the leading process is constituted by mechanical collisions within the same species. Similar results were obtained in [15] in the presence of a reversible bimolecular reaction

$$A_1 + A_2 \rightleftarrows A_3 + A_4 \,, \tag{1}$$

starting from the simplified reactive kinetic model [16], in which non–translational degrees of freedom are neglected. A nice feature of the above kinetic derivations is that non–homogeneous source terms contributed by collision operators for reactive events and/or state transitions (making equations non–conservative) emerge naturally and consistently as suitable integrals of the microscopic interaction parameters, namely the differential cross sections $\sigma(g, \cos\chi)$, or collision kernels $B(g, \cos\chi) = g\,\sigma(g, \cos\chi)$, where $g = |\mathbf{v} - \mathbf{w}|$ is the relative speed of the two molecules impinging at velocities $\mathbf{v}$ and $\mathbf{w}$, and χ the deflection angle. An unfortunate fact is that it seems hopeless casting such source terms in closed analytical form, even for the most idealized simplified collision models, like the Maxwellian molecules [2].

On the other hand, recent results from rational thermodynamics indicate that there are physical situations in which the mechanical relaxation time is shorter than the thermal one [9], or, in other words, equalization of species velocities (vanishing of diffusion velocities) is faster than equalization of temperatures, so that an adequate Euler description is provided by consideration of a single mass velocity for the gas mixture, and of different temperatures for each species. It was also shown that the thermal problem can be separated from the mechanical one for a mixture at rest [17]. Indeed, as early as 1946, Landau showed that this faster mechanical relaxation is true for plasmas [18], so that in many cases one can regard the velocities of electrons and ions as equal, whereas the temperatures are different.

It is just the above physical regime that will be addressed here, by specializing the hydrodynamic limit of the reactive Boltzmann equations worked out in [15] to the pertinent one–velocity multi–temperature frame. In this case, collision contributions in the reactive Euler equations due to the slow interactions (mechanical scattering between different species and chemical reaction) are amenable, at least for Maxwellian molecules, to exact, though cumbersome, analytical expressions, making explicit their dependence on the relevant hydrodynamic variables. The obtained fluid–dynamic model equations are then applied to one of the most classical test problems in the field, i.e. the one–dimensional steady shock wave problem, generalizing thus to the multi–temperature scenario the results achieved in [19]. Occurrence of reactive encounters changes quite drastically the

situation with respect to the analogous problem for the inert mixture, since, at the kinetic level, the relevant collision operators exhibit different collision invariants, thus different conservation equations are in order, and also a crucial parameter like the Mach number is changed, and becomes smaller than the corresponding inert one [20].

The paper is organized as follows. After recalling the main features of the reactive Boltzmann equations for a mixture of gases undergoing reaction (1), the derivation of the considered multi–temperature Euler closure is presented in Section 2, where also the various exchange rates for the quantities not conserved by the dominant process are worked out explicitly under Maxwell–like collision models for both mechanical and chemical encounters. Steady shock profiles are then analyzed in Section 3 in terms of the achieved hydrodynamic equations, going through conservation laws and Rankine–Hugoniot conditions, and reducing the problem to a four–dimensional dynamical system. Occurrence of either smooth or discontinuous solutions, and of possible relevant bifurcations versus the Mach number, are also discussed here. Indeed we observe formation of subshocks (discontinuous solutions) for varying parameters, in agreement with a famous general theorem on hyperbolic systems of balance laws rigorously proved in [21]. Our results, though obtained by a different approach, are in fact equivalent to the conditions for non–existence of smooth solutions established by Boillat and Ruggeri. Some outputs from the extensive numerical investigations for varying parameters are finally presented and commented on in Section 4.

2 Reactive multi–temperature fluid–dynamic equations

Assuming that fast collisions driving the overall evolution are elastic encounters between particles of the same species, the set of integro–differential Boltzmann–like equations governing the distribution functions $f_i(t, \mathbf{x}, \mathbf{v}) \in L^1(\mathbb{R}\times\mathbb{R}^3\times\mathbb{R}^3)$ of the considered mixture reads as

$$\frac{\partial f_i}{\partial t} + \mathbf{v}\cdot\nabla_{\mathbf{x}} f_i = \frac{1}{\varepsilon} I_{ii}[f_i, f_i] + \sum_{j\neq i} I_{ij}[f_i, f_j] + J_i[\underset{\sim}{f}] \qquad i = 1, \ldots, 4, \tag{2}$$

where $\underset{\sim}{f} = (f_1, f_2, f_3, f_4)$, I_{ij} is the collision integral for mechanical encounters of the (i, j) pair, and J_i is the net gain by collision for species i in the chemical reaction (i, j, h, k), with admissible sequences $(1, 2, 3, 4)$, $(2, 1, 4, 3)$, $(3, 4, 1, 2)$, $(4, 3, 2, 1)$. They are given by five fold integrals involving the collision kernels for pair elastic scattering B_{ij}, and the collision kernel for the direct reaction B_{12}^{34} (the one for the reverse reaction B_{34}^{12} follows by microreversibility). Each species is endowed with an energy of chemical link E_i, and the heat of reaction is given by

$$\Delta E = -\sum_{i=1}^{4} \Lambda_i E_i \qquad \underset{\sim}{\Lambda} = (1, 1, -1, -1) \tag{3}$$

in terms of the stoichiometric coefficients Λ_i. Being only matter of convention, we may always assume $\Delta E > 0$, so that an energetic threshold occurs for the direct reaction

in (1). The case $\Delta E = 0$ is very particular and quite unphysical, and will be briefly commented on at the end of Section 3. Possible activation energies are included in the collision kernels. Chemical reaction (1) implies that particle masses m_i are such that $m_1 + m_2 = m_3 + m_4$. The interested reader is referred to [15, 16] for more details, especially on collision equilibria and entropy dissipation. The former are provided by local Maxwellians at common velocity $\mathbf{u}$ and temperature T, with number densities n_i related by the so–called mass action law of chemical equilibrium

$$\frac{n_1 n_2}{n_3 n_4} = \frac{\chi_1 \chi_2}{\chi_3 \chi_4} = \left(\frac{\mu_{12}}{\mu_{34}}\right)^{3/2} \exp\left(\frac{\Delta E}{T}\right), \tag{4}$$

where $\mu_{ij} = \frac{m_i m_j}{m_i + m_j}$ denotes reduced mass, and $\chi_i = \frac{n_i}{n}$ concentration fraction with respect to total number density n. Macroscopic parameters for species and for the mixture, including pressure tensor and heat flux, are defined in the standard way (see for instance [11]). The H–theorem holds in terms of the reactive version of the classical H–functional [16]. The symbol $\varepsilon > 0$ in (2) is a kind of Knudsen number, the small parameter representing the ratio of the fast to the slow time (and length) scales, which goes to zero in the asymptotic procedure leading to the sought fluid–dynamics. We are concerned here only with the zero–order approximation, and with the closure of the macroscopic "conservation" equations relevant to the dominant operator only, labelled by $1/\varepsilon$ in (2). They are proper weak forms of (2) themselves, in number of 20, corresponding to test functions which represent particle number, momentum, and kinetic energy in each species, and are actually only balance equations, due to the contributions of the slow collision mechanisms, which do not preserve all of those quantities. In fact, the actual conservations holding for the gas as a whole are only seven, and correspond to particle number in three independent pairs of species, to the overall momentum vector, and to the overall (kinetic plus chemical) energy. This is due to the occurrence of exchanges between different species and of transformation of energy from its kinetic to its chemical form and vice versa. Since in each direct reaction of type (1) the disappearance of two particles of species 1, 2 is compensated by the appearance of two particles of species 3, 4, and vice versa in the reverse reaction, three independent sums of number densities preserved during the evolution are $n^1 + n^3$, $n^1 + n^4$, $n^2 + n^4$, but other options could be equivalently adopted. The 20 balance equations above are of course exact, but not closed in the main macroscopic fields, and obviously suitable combinations of them reproduce the actual 7 conservation equations holding for the mixture. Setting $\mathbf{g} = \mathbf{v} - \mathbf{w} = g\,\hat{\mathbf{n}}$, $r_{ij} = m_i/(m_i + m_j)$,

$$\mathbf{v}_{ij} = r_{ij}\,\mathbf{v} + r_{ji}\,(\mathbf{w} + g\,\hat{\mathbf{n}}'), \qquad \mathbf{v}_{ij}^{hk} = r_{ij}\,\mathbf{v} + r_{ji}\,\mathbf{w} + r_{kh}\,g_{ij}^{hk}\,\hat{\mathbf{n}}', \tag{5}$$

and

$$g_{ij}^{hk} = \left[\frac{\mu_{ij}}{\mu_{hk}}\left(g^2 - \delta_{ij}^{hk}\right)\right]^{1/2}, \qquad \delta_{ij}^{hk} = 2\,\frac{E_h + E_k - E_i - E_j}{\mu_{ij}}, \tag{6}$$

the general weak forms of collision operators corresponding to a smooth test function $\varphi_i(\mathbf{v})$ may be cast as

$$\int \varphi_i(\mathbf{v})\, I_{ij}[f_i, f_j](\mathbf{v})\, d_3\mathbf{v} = \iiint B_{ij}(g, \hat{\mathbf{n}} \cdot \hat{\mathbf{n}}')\Big[\varphi_i(\mathbf{v}_{ij}) - \varphi_i(\mathbf{v})\Big] f_i(\mathbf{v})\, f_j(\mathbf{w})\, d_3\mathbf{v}\, d_3\mathbf{w}\, d_2\hat{\mathbf{n}}' \tag{7}$$

and

$$\int \varphi_i(\mathbf{v})\, J_i[\underset{\sim}{f}](\mathbf{v})\, d_3\mathbf{v} = \iiint \varphi_i(\mathbf{v}_{hk}^{ij}) U(g^2 - \delta_{hk}^{ij})$$
$$\times \left(\frac{\mu_{ij}}{\mu_{hk}}\right)^{3/2} \left(1 + \frac{\mu_{ij}}{\mu_{hk}}\, \frac{\delta_{ij}^{hk}}{g^2}\right)^{1/2} B_{ij}^{hk}(g_{hk}^{ij}, \hat{\mathbf{n}} \cdot \hat{\mathbf{n}}') f_h(\mathbf{v})\, f_k(\mathbf{w})\, d_3\mathbf{v}\, d_3\mathbf{w}\, d_2\hat{\mathbf{n}}' \tag{8}$$
$$- \iiint \varphi_i(\mathbf{v})\, U(g^2 - \delta_{ij}^{hk}) B_{ij}^{hk}(g, \hat{\mathbf{n}} \cdot \hat{\mathbf{n}}') f_i(\mathbf{v})\, f_j(\mathbf{w})\, d_3\mathbf{v}\, d_3\mathbf{w}\, d_2\hat{\mathbf{n}}',$$

where U stands for unit step function. We refer once more to the quoted literature, in particular to [15], for more quantitative information.

Now the sought Euler closure is achieved, for the considered physical scenario (one–velocity, four–temperature description), by substituting the local Maxwellians

$$M_i(\mathbf{v}) = n_i \left(\frac{m_i}{2\pi T_i}\right)^{3/2} \exp\left[-\frac{m_i}{2T_i}(\mathbf{v} - \mathbf{u})^2\right] \qquad i = 1, \ldots, 4 \tag{9}$$

for the distribution functions in the set of exact balance equations discussed above. The 11 scalar parameters n_i, $\mathbf{u}$, T_i appearing in the family (9) of Gaussians are the hydrodynamic unknown fields of interest to be determined. The substitution defined by (9) greatly simplifies the exact balance equations, especially in the integrals expressing slow collision contributions, all of the type (7) and (8). Skipping again the heaviest (and the simplest) technical details, the closure procedure proceeds along the following steps.

In the selection of the 11 Euler equations it is convenient to choose the 7 fluid–dynamic equations which are naturally in conservative form, namely, as previously stated,

$$\begin{aligned}
&\frac{\partial}{\partial t}(n_i + n_j) + \nabla_{\mathbf{x}} \cdot \big[(n_i + n_j)\mathbf{u}\big] = 0 \qquad (i,j) = (1,3),\ (1,4),\ (2,4) \\
&\frac{\partial}{\partial t}(\rho\mathbf{u}) + \nabla_{\mathbf{x}} \cdot (\rho\mathbf{u} \otimes \mathbf{u}) + \nabla_{\mathbf{x}}(nT) = \mathbf{0} \\
&\frac{\partial}{\partial t}\left(\frac{1}{2}\rho u^2 + \frac{3}{2}nT + \sum_{i=1}^{4} E_i n_i\right) + \nabla_{\mathbf{x}} \cdot \left[\left(\frac{1}{2}\rho u^2 + \frac{5}{2}nT + \sum_{i=1}^{4} E_i n_i\right)\mathbf{u}\right] = 0\,,
\end{aligned} \tag{10}$$

with $n = \sum_{i=1}^{4} n_i$, $\rho = \sum_{i=1}^{4} m_i n_i$, and $nT = \sum_{i=1}^{4} n_i T_i$. We need then four equations of non–conservative type, and we may resort to the continuity equation for one single species and to the separate (kinetic) energy equations for three different species. Precisely, we choose the continuity equation for species 1 and energy equations for species 2, 3, 4, but of course other options would be equivalent:

$$\begin{aligned}
&\frac{\partial n_1}{\partial t} + \nabla_{\mathbf{x}} \cdot (n_1\mathbf{u}) = Q_1^{\mathsf{ch}} \\
&\frac{\partial}{\partial t}\left(\frac{1}{2}\rho_i u^2 + \frac{3}{2}n_i T_i\right) + \nabla_{\mathbf{x}} \cdot \left[\left(\frac{1}{2}\rho_i u^2 + \frac{5}{2}n_i T_i\right)\mathbf{u}\right] = \sum_{j \neq i} S_{ij}^{\mathsf{me}} + S_i^{\mathsf{ch}} \qquad i = 2, 3, 4,
\end{aligned} \tag{11}$$

where

$$Q_i^{\mathsf{ch}} = \int J_i\, d_3\mathbf{v}\,, \qquad S_{ij}^{\mathsf{me}} = \int \frac{1}{2} m_i v^2 I_{ij}\, d_3\mathbf{v}\,, \qquad S_i^{\mathsf{ch}} = \int \frac{1}{2} m_i v^2 J_i\, d_3\mathbf{v}\,, \tag{12}$$

with

$$Q_i^{\mathsf{ch}} = \Lambda_i Q_1^{\mathsf{ch}}\,, \qquad \sum_{i=1}^{4}\sum_{j\neq i} S_{ij}^{\mathsf{me}} = 0\,, \qquad \sum_{i=1}^{4} S_i^{\mathsf{ch}} = -\,Q_1^{\mathsf{ch}}\Delta E\,. \tag{13}$$

The source terms on the right hand side of (11) are in principle known functions of the hydrodynamic fields n_i, $\mathbf{u}$, T_i once the approximation (9) is used in (7) and (8) in order to express (12). The product of two Maxwellians of type (9) may be rewritten as

$$M_i(\mathbf{v})M_j(\mathbf{w}) = n_i n_j \left(\frac{m_i}{2\pi T_i}\right)^{3/2}\left(\frac{m_j}{2\pi T_j}\right)^{3/2} \exp\Big[-\alpha_{ij}\big(\mathbf{G}_{ij}+\gamma_{ij}\mathbf{g}-\mathbf{u}\big)^2\Big]\exp\big(-\beta_{ij}g^2\big) \tag{14}$$

with $\mathbf{G}_{ij} = r_{ij}\mathbf{v} + r_{ji}\mathbf{w}$ and

$$\alpha_{ij} = \frac{m_i}{2T_i} + \frac{m_j}{2T_j}\,, \qquad \beta_{ij} = \left(\frac{2T_i}{m_i}+\frac{2T_j}{m_j}\right)^{-1}, \qquad \gamma_{ij} = \frac{\mu_{ij}}{\alpha_{ij}}\left(\frac{1}{2T_i}-\frac{1}{2T_j}\right), \tag{15}$$

so that all integrations may be performed in terms of center of mass and relative velocities. In addition

$$(v_{ij}^{hk})^2 = G_{ij}^2 + r_{kh}^2 (g_{ij}^{hk})^2 + 2 r_{kh} g_{ij}^{hk}\mathbf{G}_{ij}\cdot\hat{\mathbf{n}}' \tag{16}$$

and analogously for v_{ij}^2, so that all angular integrations needed may be performed separately, and can be cast in terms of the quantities

$$\begin{aligned} B_{ij}^k(g) &= \int_{S^2} (\hat{\mathbf{n}}\cdot\hat{\mathbf{n}}')^k B_{ij}(g,\hat{\mathbf{n}}\cdot\hat{\mathbf{n}}')d_2\hat{\mathbf{n}}' \qquad k=0,1,\\ B_k(g) &= \int_{S^2} (\hat{\mathbf{n}}\cdot\hat{\mathbf{n}}')^k B_{12}^{34}(g,\hat{\mathbf{n}}\cdot\hat{\mathbf{n}}')d_2\hat{\mathbf{n}}' \qquad k=0,1, \end{aligned} \tag{17}$$

with $0<|B_{ij}^1|<B_{ij}^0$ and $0<|B_1|<B_0$. We set for future use $\bar{B}_{ij}(g) = B_{ij}^0(g) - B_{ij}^1(g)$. So, for instance, the reaction rate for species 1 takes the form

$$\begin{aligned} Q_1^{\mathsf{ch}} &= \left(\frac{\mu_{12}}{\mu_{34}}\right)^{3/2}\iint B_0(g_{34}^{12})\left(1+\frac{2\Delta E}{\mu_{34}g^2}\right)^{1/2} M_3(\mathbf{v})M_4(\mathbf{w})\,d_3\mathbf{G}_{34}\,d_3\mathbf{g}\\ &- \iint B_0(g)\,U\left(g^2-\frac{2\Delta E}{\mu_{12}}\right) M_1(\mathbf{v})M_2(\mathbf{w})\,d_3\mathbf{G}_{12}\,d_3\mathbf{g}\,, \end{aligned} \tag{18}$$

where also integrations with respect to center of mass velocities can be performed separately, leaving only in conclusion a scalar integral with respect to g, whose integrand depends of course on the trend of B_0 versus g. Analogous steps apply to the mechanical energy exchange rates, with final result

$$S_{ij}^{\mathsf{me}} = -\,\mu_{ij}\iint \bar{B}_{ij}(g)\mathbf{G}_{ij}\cdot\mathbf{g}\,M_i(\mathbf{v})M_j(\mathbf{w})\,d_3\mathbf{G}_{ij}\,d_3\mathbf{g}\,. \tag{19}$$

The chemical energy exchange rate

$$\begin{aligned} S_i^{\mathsf{ch}} &= \frac{1}{2}m_i\left(\frac{\mu_{ij}}{\mu_{hk}}\right)^{3/2}\iiint (v_{hk}^{ij})^2 U(g^2-\delta_{hk}^{ij})\left(1+\frac{\mu_{ij}}{\mu_{hk}}\frac{\delta_{ij}^{hk}}{g^2}\right)^{1/2}\\ &\times\; B_{ij}^{hk}(g_{hk}^{ij},\hat{\mathbf{n}}\cdot\hat{\mathbf{n}}')M_h(\mathbf{v})M_k(\mathbf{w})d_3\mathbf{G}_{hk}\,d_3\mathbf{g}\,d_2\hat{\mathbf{n}}'\\ &-\; \frac{1}{2}m_i\iiint v^2 U(g^2-\delta_{ij}^{hk})B_{ij}^{hk}(g,\hat{\mathbf{n}}\cdot\hat{\mathbf{n}}')M_i(\mathbf{v})M_j(\mathbf{w})\,d_3\mathbf{G}_{ij}\,d_3\mathbf{g}\,d_2\hat{\mathbf{n}}' \end{aligned} \tag{20}$$

can be handled in the same way, after resorting to (16), to the result

$$\int_{S^2} \hat{\mathbf{n}}'\, B_{ij}^{hk}(\xi, \hat{\mathbf{n}}\cdot\hat{\mathbf{n}}')d_2\hat{\mathbf{n}}' = \frac{1}{g}\,\mathbf{g}\int_{S^2}(\hat{\mathbf{n}}\cdot\hat{\mathbf{n}}')B_{ij}^{hk}(\xi, \hat{\mathbf{n}}\cdot\hat{\mathbf{n}}')d_2\hat{\mathbf{n}}'\,, \tag{21}$$

to definitions (17), and to microreversibility relation

$$B_{34}^{12}(g, \hat{\mathbf{n}}\cdot\hat{\mathbf{n}}') = \left(\frac{\mu_{12}}{\mu_{34}}\right)^2 \frac{g_{34}^{12}}{g}\, B_{12}^{34}(g_{34}^{12}, \hat{\mathbf{n}}\cdot\hat{\mathbf{n}}')\,. \tag{22}$$

We omit for brevity the huge final expression, also because it is not needed for the purpose of the present work. We shall rather concentrate on a case in which all of the above integrations can be cast in closed analytical form, namely the Maxwell collision model

$$B_{ij}(g, \hat{\mathbf{n}}\cdot\hat{\mathbf{n}}') = \varkappa_{ij}(\hat{\mathbf{n}}\cdot\hat{\mathbf{n}}'), \qquad\qquad B_{12}^{34}(g, \hat{\mathbf{n}}\cdot\hat{\mathbf{n}}') = \varkappa(\hat{\mathbf{n}}\cdot\hat{\mathbf{n}}'), \tag{23}$$

in which case all of the B_{ij}^k, $\bar{B}_{ij}$, B_k become some constant $\varkappa_{ij}^k$, $\bar{\varkappa}_{ij}$, $\varkappa_k$, while the collision kernel for the reverse reaction exhibits a dependence on the relative speed

$$B_{34}^{12}(g, \hat{\mathbf{n}}\cdot\hat{\mathbf{n}}') = \left(\frac{\mu_{12}}{\mu_{34}}\right)^{3/2}\left(1+\frac{2\Delta E}{\mu_{34}g^2}\right)^{1/2}\varkappa(\hat{\mathbf{n}}\cdot\hat{\mathbf{n}}'). \tag{24}$$

Under option (23), in contribution (19) the quantity $\bar{B}_{ij}$ is constant hence it comes out of the integral, and bearing in mind the expression (14) for $M_i(\mathbf{v})M_j(\mathbf{w})$ the integrations over the variables $\mathbf{G}_{ij}$ and $\mathbf{g}$ may be performed separately, leading to

$$S_{ij}^{\mathsf{me}} = -\,3r_{ij}r_{ji}n_in_j\bar{\varkappa}_{ij}(T_i - T_j). \tag{25}$$

Lengthier but rather standard manipulations allow to reduce (18) to Gaussian integrals on cut domains, leading to the appearance of incomplete Euler gamma functions of half integer order (amenable to error functions). They yield

$$\begin{aligned} Q_1^{\mathsf{ch}} \;&=\; \frac{2}{\sqrt{\pi}}\,\varkappa_0\left[n_3n_4\left(\frac{\mu_{12}}{\mu_{34}}\right)^{3/2}\exp\left(\frac{\Delta E}{r_{43}T_3+r_{34}T_4}\right)\Gamma\left(\frac{3}{2},\frac{\Delta E}{r_{43}T_3+r_{34}T_4}\right)\right. \\ &-\; \left. n_1n_2\Gamma\left(\frac{3}{2},\frac{\Delta E}{r_{21}T_1+r_{12}T_2}\right)\right]. \end{aligned} \tag{26}$$

For $i=1$ (and similarly for $i=2$) the reactive energy exchange rate becomes

$$\begin{aligned} S_1^{\mathsf{ch}} \;&=\; \left(\frac{\mu_{12}}{\mu_{34}}\right)^{3/2} n_3n_4\left(\frac{m_3}{2\pi T_3}\right)^{3/2}\left(\frac{m_4}{2\pi T_4}\right)^{3/2}\frac{1}{2}\,m_1 \\ &\times\; \iint\left\{\varkappa_0\left[G_{34}^2 + r_{21}^2\frac{\mu_{34}}{\mu_{12}}\left(g^2+\frac{2\Delta E}{\mu_{34}}\right)\right]\left(1+\frac{2\Delta E}{\mu_{34}g^2}\right)^{1/2} + 2\varkappa_1 r_{21}\left(\frac{\mu_{34}}{\mu_{12}}\right)^{1/2}\right. \\ &\times\; \left.\mathbf{G}_{34}\cdot\mathbf{g}\left(1+\frac{2\Delta E}{\mu_{34}g^2}\right)\right\}\exp\Big[-\alpha_{34}\big(\mathbf{G}_{34}+\gamma_{34}\mathbf{g}-\mathbf{u}\big)^2\Big]\exp(-\beta_{34}g^2)d_3\mathbf{G}_{34}d_3\mathbf{g} \\ &-\; n_1n_2\left(\frac{m_1}{2\pi T_1}\right)^{3/2}\left(\frac{m_2}{2\pi T_2}\right)^{3/2}\frac{1}{2}m_1\varkappa_0\iint\big(\mathbf{G}_{12}+r_{21}\mathbf{g}\big)^2\,U\left(g^2-\frac{2\Delta E}{\mu_{12}}\right) \\ &\times\; \exp\Big[-\alpha_{12}\big(\mathbf{G}_{12}+\gamma_{12}\mathbf{g}-\mathbf{u}\big)^2\Big]\exp(-\beta_{12}g^2)d_3\mathbf{G}_{12}d_3\mathbf{g}\,, \end{aligned} \tag{27}$$

and again patient and careful calculations allow an explicit result in terms of incomplete gamma functions. Analogous steps are in order for S_3^{ch} (and similarly for S_4^{ch})

$$\begin{aligned}
S_3^{\mathsf{ch}} &= n_1 n_2 \left(\frac{m_1}{2\pi T_1}\right)^{3/2} \left(\frac{m_2}{2\pi T_2}\right)^{3/2} \frac{1}{2}\, m_3 \\
&\times \iint \left\{ \varkappa_0 \left[G_{12}^2 + r_{43}^2 \frac{\mu_{12}}{\mu_{34}} \left(g^2 - \frac{2\Delta E}{\mu_{12}} \right) \right] + 2\varkappa_1 r_{43} \left(\frac{\mu_{12}}{\mu_{34}}\right)^{1/2} \mathbf{G}_{12}\cdot\mathbf{g} \left(1 - \frac{2\Delta E}{\mu_{12} g^2}\right)^{1/2} \right\} \\
&\times U\left(g^2 - \frac{2\Delta E}{\mu_{12}}\right) \exp\Big[-\alpha_{12}\big(\mathbf{G}_{12} + \gamma_{12}\mathbf{g} - \mathbf{u}\big)^2 \Big] \exp(-\beta_{12} g^2) d_3\mathbf{G}_{12} d_3\mathbf{g} \\
&- \left(\frac{\mu_{12}}{\mu_{34}}\right)^{3/2} n_3 n_4 \left(\frac{m_3}{2\pi T_3}\right)^{3/2} \left(\frac{m_4}{2\pi T_4}\right)^{3/2} \frac{1}{2} m_3 \varkappa_0 \iint \big(\mathbf{G}_{34} + r_{43}\mathbf{g}\big)^2 \left(1 + \frac{2\Delta E}{\mu_{34} g^2}\right)^{1/2} \\
&\times \exp\Big[-\alpha_{34}\big(\mathbf{G}_{34} + \gamma_{34}\mathbf{g} - \mathbf{u}\big)^2 \Big] \exp(-\beta_{34} g^2) d_3\mathbf{G}_{34} d_3\mathbf{g}\,.
\end{aligned} \tag{28}$$

Skipping all intermediate details, at the end of the tedious procedure, it is possible to summarize all reactive energy rates in a single expression, featuring the stoichiometric coefficients

$$\begin{aligned}
S_i^{\mathsf{ch}} = \frac{1}{\sqrt{\pi}} m_i \varkappa_0 \Bigg\{ & \left(\frac{\mu_{ij}}{\mu_{hk}}\right)^{\frac{3(1+\Lambda_i)}{4}} n_h n_k \exp\left(\frac{(\Lambda_i+1)\Delta E}{2(r_{kh}T_h + r_{hk}T_k)}\right) \Bigg[\Bigg(\frac{3T_h T_k}{m_k T_h + m_h T_k} \\
& -(1-\Lambda_i)\frac{\mu_{ij}}{m_i^2}\Delta E - (1+\Lambda_i)\mu_{hk}\left(\frac{T_k - T_h}{m_k T_h + m_h T_k}\right)^2 \Delta E + u^2 \Bigg) \Gamma\left(\frac{3}{2}, \frac{\Delta E}{r_{kh}T_h + r_{hk}T_k}\right) \\
& +2\left(r_{kh}T_h + r_{hk}T_k\right) \left[\mu_{hk}\left(\frac{T_k - T_h}{m_k T_h + m_h T_k}\right)^2 + \frac{\mu_{ij}}{m_i^2} \right] \Gamma\left(\frac{5}{2}, \frac{\Delta E}{r_{kh}T_h + r_{hk}T_k}\right) \Bigg] - \left(\frac{\mu_{hk}}{\mu_{ij}}\right)^{\frac{3(1-\Lambda_i)}{4}} \\
& \times n_i n_j \exp\left(\frac{(1-\Lambda_i)\Delta E}{2(r_{ji}T_i + r_{ij}T_j)}\right) \Bigg[\Bigg(\frac{3T_i T_j}{m_j T_i + m_i T_j} - (1-\Lambda_i)\mu_{ij}\left[\frac{(m_i+m_j)T_i}{m_j T_i + m_i T_j}\right]^2 \Delta E + u^2 \Bigg) \\
& \times \Gamma\left(\frac{3}{2}, \frac{\Delta E}{r_{ji}T_i + r_{ij}T_j}\right) + 2\mu_{ij}\left(r_{ji}T_i + r_{ij}T_j\right) \left[\frac{(m_i+m_j)T_i}{m_j T_i + m_i T_j}\right]^2 \Gamma\left(\frac{5}{2}, \frac{\Delta E}{r_{ji}T_i + r_{ij}T_j}\right) \Bigg] \Bigg\} \\
& -2\left(\frac{\mu_{ij}}{\mu_{hk}}\right)^{\frac{1+3\Lambda_i}{4}} r_{ij} r_{ji} n_h n_k \varkappa_1 \exp\left(\frac{(\Lambda_i - 1)\Delta E}{2(r_{kh}T_h + r_{hk}T_k)}\right) \left(\frac{3}{2} + \frac{\Delta E}{r_{kh}T_h + r_{hk}T_k}\right) (T_k - T_h)\,.
\end{aligned} \tag{29}$$

For Maxwell type collision model (23), the multi–temperature single–velocity Euler equations for reaction (1) are then given by the 11 equations (10)+(11), with exchange rates for non–conserved quantities provided by (25), (26), and (29) in terms of the angle–integrated constant collision kernels $\bar{\varkappa}_{ij}$, $\varkappa_0$, and $\varkappa_1$.

"Collision" equilibria for such a set of evolution equations correspond to states for which all reactive rates on the right hand sides vanish. The "physical" equilibrium from kinetic theory requires all equal temperatures and mass action law (4) for densities and temperature. It is readily seen that $T_i = T_j\ \forall i,j$ implies immediately $S_{ij}^{\mathsf{me}} = 0\ \forall i,j$, and

$$Q_1^{\mathsf{ch}} = \frac{2}{\sqrt{\pi}}\, \varkappa_0 \Gamma\left(\frac{3}{2}, \frac{\Delta E}{T}\right) \left[n_3 n_4 \left(\frac{\mu_{12}}{\mu_{34}}\right)^{3/2} \exp\left(\frac{\Delta E}{T}\right) - n_1 n_2 \right]. \tag{30}$$

Moreover, all S_i^{ch} are proportional to Q_1^{ch}, for instance

$$\begin{aligned} S_1^{\mathsf{ch}} &= \frac{1}{\sqrt{\pi}}\, m_1 \varkappa_0 \left[\left(\frac{3T}{m_1+m_2} + u^2 \right) \Gamma\left(\frac{3}{2}, \frac{\Delta E}{T} \right) + \frac{2m_2 T}{m_1(m_1+m_2)} \Gamma\left(\frac{5}{2}, \frac{\Delta E}{T} \right) \right] \\ &\times \left[n_3 n_4 \left(\frac{\mu_{12}}{\mu_{34}} \right)^{3/2} \exp\left(\frac{\Delta E}{T} \right) - n_1 n_2 \right]. \end{aligned} \tag{31}$$

If then (4) holds, all Q_i^{ch} and S_i^{ch} are bound to vanish, as expected from any good approximation. Actually, if we pretend collision equilibria to hold for any choice of (Maxwellian) collision kernels, the above "physical" equilibria are in a sense unique. In fact, mechanical and reactive collision contributions should then vanish simultaneously, and, due to negativity properties of the matrix appearing in S_{ij}^{me}, established in [15], this requires that all temperatures must be equal to each other. Once we can rely on this statement, the reactive collision contributions take forms (30), (31), and must in turn vanish, which happens if and only if the mass action law (4) holds.

Option (23) is not the only one allowing an analytical form of exchange rates, even simpler expressions would arise if instead the exothermic collision kernel B_{34}^{12} were taken independent of g, and some simple power like trend could be worked out at the price of additional machinery. For the application presented below in this paper we shall stick to (23), which is simple enough for calculations, and at the same time realistic enough to represent a typical threshold event, with a microscopic collision frequency shaped as a perfect step.

3 Application to the one–dimensional shock wave problem

As anticipated, we shall test the reactive multi–temperature fluid–dynamic Euler model proposed in the previous section on the classical steady shock problem in one space dimension, in which case mass velocity becomes a scalar, and we are left with 9 observable fields, governed, in the reference frame of the moving wave, by the set of ordinary differential equations

$$\begin{aligned} &\frac{d}{dx}(n_1 u) = Q_1^{\mathsf{ch}} \\ &\frac{d}{dx}\big[(n_i + n_j)u\big] = 0 \qquad\qquad (i,j) = (1,3),\ (1,4),\ (2,4) \\ &\frac{d}{dx}\big(\rho u^2 + nT\big) = 0 \\ &\frac{d}{dx}\left(\frac{1}{2}\rho u^3 + \frac{5}{2} nTu + \sum_{i=1}^{4} E_i n_i u \right) = 0 \\ &\frac{d}{dx}\left(\frac{1}{2}\rho_i u^3 + \frac{5}{2} n_i T_i u \right) = \sum_{j\neq i} S_{ij}^{\mathsf{me}} + S_i^{\mathsf{ch}} \qquad\qquad i = 2,3,4, \end{aligned} \tag{32}$$

where Q_1^{ch}, S_{ij}^{me}, and S_i^{ch} are given respectively by (26), (25), and (29). The shock solution must join two limiting equilibrium states at $x \to \pm\infty$, which are then characterized by

$$T_i^{\pm} = T^{\pm} \qquad i = 1, \ldots, 4, \qquad\qquad \frac{\chi_1^{\pm}\chi_2^{\pm}}{\chi_3^{\pm}\chi_4^{\pm}} = \left(\frac{\mu_{12}}{\mu_{34}}\right)^{3/2} \exp\left(\frac{\Delta E}{T^{\pm}}\right). \tag{33}$$

Each state is then determined by the knowledge (for instance) of density $n^{\pm}$, temperature $T^{\pm}$, two out of the four concentration fractions $\chi_i^{\pm}$, and velocity $u^{\pm}$, which also define the relevant sound speeds via [20]

$$c^{\pm} = \alpha^{\pm}\left(\frac{5n^{\pm}T^{\pm}}{3\rho^{\pm}}\right)^{1/2} \qquad\qquad (\alpha^{\pm})^2 = \frac{\displaystyle\sum_{i=1}^{4}\frac{1}{\chi_i^{\pm}} + \frac{2}{5}\left(\frac{\Delta E}{T^{\pm}}\right)^2}{\displaystyle\sum_{i=1}^{4}\frac{1}{\chi_i^{\pm}} + \frac{2}{3}\left(\frac{\Delta E}{T^{\pm}}\right)^2} < 1\,, \tag{34}$$

and the corresponding Mach numbers

$$\mathsf{Ma}^{\pm} = \frac{u^{\pm}}{c^{\pm}}\,. \tag{35}$$

The 5 conservation laws in (32) establish a relation between the 5 downstream (+) and upstream (−) parameters, the famous Rankine–Hugoniot conditions, which determine the downstream state once the upstream one is given, like in the much more standard and manageable inert problem. A detailed analysis has already been performed in Ref. [20], but some steps are repeated here for the readers' convenience. Rankine–Hugoniot conditions read as

$$\begin{aligned}
&(n_i^- + n_j^-)u^- = (n_i^+ + n_j^+)u^+ \qquad (i,j) = (1,3),\ (1,4),\ (2,4),\\
&n^-T^- + \rho^-(u^-)^2 = n^+T^+ + \rho^+(u^+)^2,\\
&\frac{1}{2}\,\rho^-(u^-)^3 + \frac{5}{2}\,n^-T^-u^- + \sum_{i=1}^{4} E_i n_i^- u^- = \frac{1}{2}\,\rho^+(u^+)^3 + \frac{5}{2}\,n^+T^+u^+ + \sum_{i=1}^{4} E_i n_i^+ u^+;
\end{aligned} \tag{36}$$

the first three of them may be rewritten as

$$(\chi_i^- + \chi_j^-)n^-u^- = (\chi_i^+ + \chi_j^+)n^+u^+ \qquad (i,j) = (1,3),\ (1,4),\ (2,4), \tag{37}$$

and simple manipulations show that

$$\chi_i^+ = \chi_i^- + \Lambda_i\Delta\chi \qquad i = 1, \ldots, 4, \qquad\qquad \frac{n^+}{n^-} = \frac{\rho^+}{\rho^-} = \frac{u^-}{u^+}\,, \tag{38}$$

where the parameter $\Delta\chi$ is proved to be in a one–to–one relationship with u^- and then with the upstream Mach number, and determines uniquely T^+ via (33). The process is then closed by the formulas

$$\begin{aligned}
&\frac{n^+}{n^-} = 2\left(1 - \frac{T^-}{T^+}\right) - \frac{\Delta E}{T^+}\Delta\chi + \left\{\left[2\left(1 - \frac{T^-}{T^+}\right) - \frac{\Delta E}{T^+}\Delta\chi\right]^2 + \frac{T^-}{T^+}\right\}^{1/2}\\
&u^- = \left(\frac{n^-T^-}{\rho^-}\right)^{1/2}\left[\frac{n^+}{n^-}\,\frac{1 - (n^+/n^-)(T^+/T^-)}{1 - (n^+/n^-)}\right]^{1/2}.
\end{aligned} \tag{39}$$

Finally, the entropy flux condition imposed by the H–theorem results in the constraint, to be fulfilled for a physical shock wave to exist, $\Delta\chi < 0$, which is equivalent to the familiar $\mathsf{Ma}^- > 1$.

When solving the differential set (32), the 5 conservation equations allow to eliminate 5 variables, namely all n_i and T, in terms of u, explicitly

$$\begin{aligned} n_i &= \frac{n_i^- u^-}{u} - \Lambda_i N \qquad\qquad T = \frac{\rho^-(u^-)^2 + n^- T^-}{n^- u^-}\, u - \frac{\rho^-}{n^-}\, u^2 \\ N &= \frac{1}{\Delta E}\left[2\rho^- u^- u - \frac{5}{2}\big(\rho^-(u^-)^2 + n^- T^-\big) + \left(\frac{1}{2}\,\rho^-(u^-)^3 + \frac{5}{2}\, n^- T^- u^-\right)\frac{1}{u}\right], \end{aligned} \tag{40}$$

implying also $n = n^- u^-/u$ and $\rho = \rho^- u^-/u$. Since also $nT = \sum_{i=1}^4 n_i T_i$, we are left with only 4 unknown fields, namely u, T_2, T_3, T_4, for which we have to solve the 4 non–conservative equations in (32), that could be cast in normal form to yield the four–dimensional dynamical system to be solved numerically, looking for an heteroclinic orbit connecting the upstream and downstream equilibria in the phase space. The crucial problem is the first equation, which reduces to the form

$$\frac{d}{dx}F(u) = G(u, T_2, T_3, T_4), \qquad\qquad \lim_{x\to\pm\infty} u(x) = u^\pm, \tag{41}$$

where G is nothing but Q_1^{ch}, which depends on all n_i and T_i, once variables have been reduced by the use of (40), while $F = n_1 u$ takes the polynomial form in u

$$F(u) = n_1^- u^- - \frac{1}{\Delta E}\left[2\rho^- u^- u^2 - \frac{5}{2}\big(\rho^-(u^-)^2 + n^- T^-\big)u + \frac{1}{2}\,\rho^-(u^-)^3 + \frac{5}{2}\, n^- T^- u^-\right]. \tag{42}$$

The derivative $F'(u) = \frac{dF}{du}$ is then linear in u, and vanishes at $u = u^*$, where

$$u^* = \frac{5}{8}\,\frac{\rho^-(u^-)^2 + n^- T^-}{\rho^- u^-}\,, \tag{43}$$

so that the vector field of the dynamical system is singular on the hyperplane $u = u^*$, which might or might not interfere with the admissible phase space. It is easy to check that in our problem we have $0 < u^+ < u^-$, and that the collocation of u^* with respect to u^- is represented by

$$u^* \gtrless u^- \quad \Longleftrightarrow \quad (u^-)^2 \lesseqgtr \frac{5n^- T^-}{3\rho^-} \quad \Longleftrightarrow \quad \mathsf{Ma}^- \lesseqgtr \frac{1}{\alpha^-}\,. \tag{44}$$

We deduce that for slightly supersonic flows (upstream Mach number in the interval $(1, 1/\alpha^-)$) one can expect that the singularity does not affect the phase space, the vector field is regular, and a smooth solution for the steady shock is allowed. But, as soon as u^- increases and the Mach number exceeds the threshold $1/\alpha^- > 1$, a smooth solution is ruled out, and one has to search for weak solutions, presenting jump discontinuity, which indeed are the only possible shock solutions for the standard (conservative) inert Euler equations. This effect is not new in classical thermodynamics [22]: though the equations are of Euler type, there is a small region in parameter space in which non–equilibrium

processes (like chemical reactions) have a dissipative effect, similar to viscosity or heat conduction, and allow for a smooth solution, whereas in most of that space the solution necessarily presents a discontinuity. The transition from one regime to the other occurs here at the bifurcation value $1/\alpha^-$ of the Mach number. Similar (stronger) dissipative effects are expected to occur in a multi–velocity and multi–temperature Euler approach, because of the presence of diffusion velocities for the various species, which also induce non–vanishing viscous stress and heat flux for the mixture, though single distribution functions are Maxwellians. However, the problem, which requires much heavier numerical computations, is not addressed here, and will be considered in future investigations.

In order to study weak solutions with discontinuity at some point x (that can be always shifted by invariance to the origin), one has to look for a piecewise smooth solution in the separate intervals $(-\infty, 0)$ and $(0, +\infty)$, satisfying limiting conditions at $\pm\infty$, and whose limits for $x \to 0^-$ and $x \to 0^+$, labelled by m and p superscripts, respectively, fulfil the constraints following from the differential equations themselves. Since the right hand sides of the last three equations in (32) are bounded functions, those equations imply merely continuity of the quantities under derivative operator across the jump, namely

$$\frac{1}{2}\,\rho_i^m (u^m)^3 + \frac{5}{2}\,n_i^m T_i^m u^m = \frac{1}{2}\,\rho_i^p (u^p)^3 + \frac{5}{2}\,n_i^p T_i^p u^p \qquad i = 2, 3, 4. \tag{45}$$

This is not true for the velocity field, as follows from (41), since $F'(u)$ vanishes at $u = u^*$. However, the same technique as before yields the constraint $F(u^m) = F(u^p)$, from which, on using (42) and bearing (43) in mind

$$\frac{u^p + u^m}{2} = \frac{5}{8}\,\frac{\rho^-(u^-)^2 + n^- T^-}{\rho^- u^-} = u^*\,, \tag{46}$$

meaning that the singular value $u = u^*$ exactly represents the midpoint of any admissible jump.

The jump in the velocity profile induces of course corresponding discontinuities in the gas number density $n = n^- u^-/u$, in the temperature T, and in the species densities n^i, as prescribed by (40). There is instead no jump for the concentrations χ_i, since the single continuity equations may be written as

$$\frac{d\chi_i}{dx} = \frac{\Lambda_i}{n^- u^-}\,Q_1^{\mathsf{ch}}\,, \tag{47}$$

where now the right hand side is a bounded function of x. So, the same reasoning leading to (45) yields now $\chi_i^p = \chi_i^m$.

In order to construct the sought (smooth or weak) solutions, one needs to investigate stability of the limiting equilibria. We consider the subsystem made by the balance equations in (32), namely the first and last three equations, in the chosen unknowns u, T_2, T_3, T_4. We have rewritten it in normal form and we have studied the relevant Jacobian matrix with the help of symbolic manipulation, that was able to determine at both ends its four eigenvalues. In all cases that have been run, it turns out that all eigenvalues of the downstream state have negative real part. The same happens for the upstream state as long as $\mathsf{Ma}^- > 1/\alpha^-$ (weak solution regime). As soon as Ma^- descends below this bifurcation value (possible smooth solution), the upstream Jacobian matrix exhibits

one positive eigenvalue, while the other three keep negative real part. The transition is singular in that such an eigenvalue diverges to $-\infty$ when Ma^- approaches the threshold from above, and re–appears from $+\infty$ after the crossing. The scenario suggested by the above facts, and confirmed by numerical experiments presented in the next Section, is the following.

For $\mathsf{Ma}^- < 1/\alpha^-$ the upstream equilibrium is a saddle with a one–dimensional unstable manifold and a three–dimensional stable manifold, and the only way to reach it running backwards towards $-\infty$ is to follow the unstable manifold, tangent to the one–dimensional unstable eigenspace. That manifold represents the unique non–constant solution of our shock problem fulfilling the upstream condition, and enters the phase space, where it is attracted by the asymptotically stable downstream equilibrium, providing the sought heteroclinic orbit, and the smooth shock profile.

For $\mathsf{Ma}^- > 1/\alpha^-$ the upstream equilibrium is itself asymptotically stable, and the only admissible solution satisfying the upstream condition is the constant solution, which of course can not reach the downstream equilibrium for $x \to +\infty$. The only way to do that is through a jump discontinuity, governed by (45) and (46), where necessarily ρ_i^m, u^m, n_i^m, T_i^m must coincide with ρ_i^-, u^-, n_i^-, T_i^-. A simple calculation yields then the corresponding values reached across the jump

$$\begin{aligned} u^p &= 2u^* - u^- = \frac{\rho^-(u^-)^2 + 5n^-T^-}{4\rho^- u^-}\,, \\ T_i^p &= \frac{n_i^- u^-}{n_i^p u^p}\,T^- + \frac{1}{5}\,m_i\left(\frac{n_i^- u^-}{n_i^p u^p}(u^-)^2 - (u^p)^2\right) \qquad i = 2,3,4, \end{aligned} \tag{48}$$

where n_i^p (as well as all other quantities of interest) are determined by u^p via (40). At this point, the state (48) across the jump is a point in the phase space attracted by the asymptotically stable downstream equilibrium, and a smooth trajectory joins it to that state for $x \to +\infty$. This builds up the sought weak shock wave solution (subshock), with a jump discontinuity from upstream equilibrium to an intermediate non–equilibrium state, followed by a smooth tail leading that state to the downstream equilibrium. Actually, formation of subshocks is not observed, and not predicted at the kinetic level (see for instance [23, 24] for reactive BGK approaches). As conjectured in the inert case [8], the reason of this discrepancy could be the fact that the Euler closure neglects many dissipative effects (like viscosity and heat conductivity) and more moments are needed in order to reproduce results obtained by kinetic models for high Mach numbers.

In all of the above discussion we have implicitly assumed $\Delta E \neq 0$ (i.e., $\Delta E > 0$) and avoided particular cases. We just comment that only a constant solution is possible for $\mathsf{Ma}^- = 1$, and that for $\mathsf{Ma}^- = 1/\alpha^-$ the jump disappears, but the solution is not smooth since the initial slopes of the tails diverge. When instead $\Delta E = 0$ the shock problem even changes its nature, and, as shown in [20], only an inert–like step profile is possible, with the same chemical composition up– and downstream.

4 Results and comments

We shall show explicitly in this Section the shock profiles resulting from the numerical integration of the multi–temperature Euler differential equations (32) for the 9 fields n_i, u, T_i, $i = 1, \ldots, 4$, describing the considered gas mixture undergoing reaction (1). Such equations may be made non–dimensional by re–scaling masses, collision kernels, densities, velocities, temperatures, and the independent variable x in terms of typical values $\tilde{m}$, $\tilde{B}$, $\tilde{n}$, $\tilde{u}$, $\tilde{T}$, and L. Choosing $\tilde{T} = \Delta E$, and accordingly $\tilde{u} = (\Delta E/\tilde{m})^{1/2}$, the parameter ΔE disappears at all, and dimensionless equations differ from the dimensional ones only by the presence of a factor $\tilde{u}/\tilde{B}\tilde{n}L$ in front of the space derivatives. Therefore, the choice $L = \tilde{u}/\tilde{B}\tilde{n}$ yields a kind of universal set of equations which, just upon re–scaling, are valid for any selection of the various reference units. In conclusion, aiming mainly at illustrative and comparative purposes for varying parameters, we consider equations (32) as dimensionless, on arbitrary scales, and with ΔE implicitly understood to be unity. The relevant results are then sensitive only to the mutual relationships among masses and among collision kernels (mechanical and reactive), and to the fixed upstream conditions (in particular, the Mach number Ma^-). Smooth solutions are normalized in such a way that $u(0) = (u^+ + u^-)/2$, whereas for weak solutions the jump is located at $x = 0$. All computations were performed by integrating forward and resorting to standard Runge–Kutta methods.

As a reference test case, having in mind a possible bimolecular reaction like $H_2O + H \rightleftarrows OH + H_2$, the dimensionless masses are taken to be

$$m_1 = 1.8 \qquad m_2 = 0.1 \qquad m_3 = 1.7 \qquad m_4 = 0.2\,, \tag{49}$$

and, to begin with, collision frequencies are chosen as $\bar{\varkappa}_{ij} = 1$, $\varkappa_0 = 1$, $\varkappa_1 = 0.5$ (equally effective mechanical and reactive exchange mechanisms and forwardly oriented anisotropy). As upstream conditions we take the situation defined by $n^- = 1.85$ and by concentration fractions

$$\chi_1^- = 0.4324 \qquad \chi_2^- = 0.4865 \qquad \chi_3^- = 0.0270 \qquad \chi_4^- = 0.0541\,, \tag{50}$$

from which $T^- = 0.1688$ and $\alpha^- = 0.9421$. The bifurcation value for Ma^- is then $1/\alpha^- = 1.0614$. Now, on the basis of the Rankine–Hugoniot conditions previously discussed, both limiting conditions for the shock problem are determined by assigning the parameter $\Delta\chi < 0$, which, via the various equations (38), (33), (39), (35), defines uniquely u^- (and then Ma^-) as well as all downstream parameters n^+, χ_i^+, T^+, u^+.

An important role is played, as anticipated, by the stability properties of the upstream equilibrium, which undergoes a bifurcation when parameters are varied. The real parts of the eigenvalues, determined by using Symbolic Math Toolbox in Matlab, are plotted versus $\mathsf{Ma}^- > 1$ in Figure 1. On a physical scale (left plot), one can see how, for increasing Ma^-, there is a positive eigenvalue blowing up when approaching bifurcation, and three negative eigenvalues, two of which merge together in a complex conjugate pair with negative real part. After the critical threshold, the formerly positive eigenvalue re–appears from $-\infty$, and then increases up to the order of magnitude of the other eigenvalues, which remain negative, after "feeling" only slightly the occurrence of criticality, and seem to stabilize

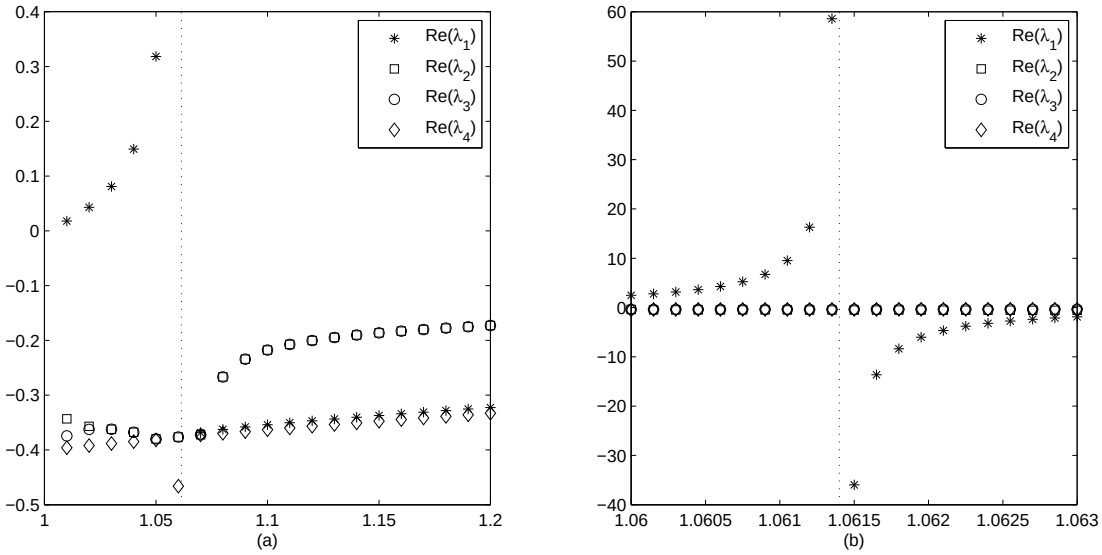

Figure 1: Real part of the eigenvalues of the upstream equilibrium for the reference case versus Mach number on a physical (a) and on a stretched (b) scale. The bifurcation value for Ma^- is marked by a dotted line.

at constant values for increasing Ma^-. On the stretched scale around the critical Mach number (right plot), one can see the very abrupt and fast variations of the bifurcating eigenvalue, occurring on the scale of the fourth significant digit; on that vertical scale all other eigenvalues appear as coincident.

We start from the choice $\mathsf{Ma}^- = 1.01$ (corresponding to $\Delta\chi = -0.0008$) and implying $u^- = 0.5369$, $u^+ = 0.5283$, $T^+ = 0.1701$. In this only slightly supersonic case, the very smooth shock profiles for u and T_i are shown in Figure 2 (notice the stretched vertical scale). The solution has been found numerically starting from a close neighborhood in phase space of the upstream equilibrium, choosing an initial point in the direction of its one–dimensional unstable eigenspace. After trials and errors, the phase trajectory leaves the neighborhood along the unstable manifold, and tends, for $x \to +\infty$, to the downstream equilibrium, which is always asymptotically stable (all eigenvalues, not shown here for brevity, have negative real parts).

We increase then Ma^- to 1.06 (very close to the bifurcation value, but still on the smooth side), corresponding to $\Delta\chi = -0.0046$. In this case $u^- = 0.5635$, $u^+ = 0.5128$, $T^+ = 0.1766$, and we plot mass velocity, gas temperature, species densities, and species temperatures in Figure 3. Trends remain of the same type, of course with stronger separation between the asymptotic values, but the much higher positive eigenvalue (see Figure 1) makes detachment from the upstream equilibrium much faster, which explains the much sharper edge and the considerable steepening of the profiles upstream, whereas the trends downstream remain more gradual (no significant changes in the eigenvalues at $+\infty$). One may notice possible occurrence of overshooting in some species temperatures.

If we now increase the Mach number across the bifurcation and take $\mathsf{Ma}^- = 1.065$ i.e. $\Delta\chi = -0.0050$ (0.5% variation), asymptotic values also change very little ($u^- = 0.5662$,

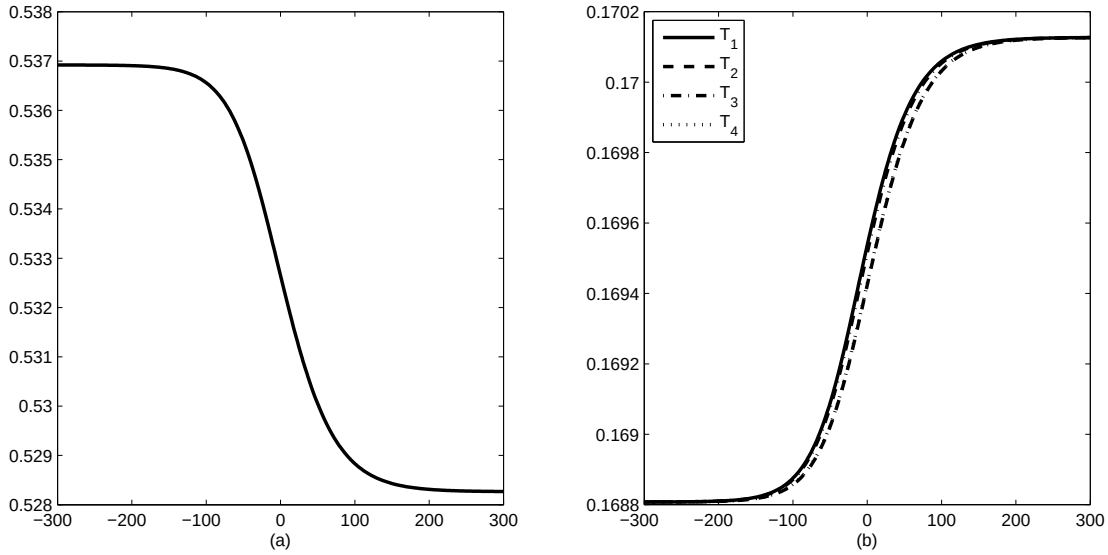

Figure 2: Mass velocity (a) and species temperatures (b) versus x for the reference case when $\mathsf{Ma}^- = 1.01$.

$u^+ = 0.5114$, $T^+ = 0.1772$) but the singularity enters the phase space ($u^* = 0.5647$), and only a discontinuous solution exists, as shown in Figure 4, as a development of the previous (smooth) sharp edge.

If Ma^- is increased further to 1.15 ($u^- = 0.6113$, $u^* = 0.5774$, $u^+ = 0.4896$) the jump discontinuity enlarges significantly (a considerable fraction of the gap between upstream and downstream states), with a clear overshooting effect for some temperatures, and a much larger spread among species across the shock front, as shown for u and the T_i in Figure 5. One can notice also some affinity in the temperatures of species with comparable mass. The same effects become more and more evident for increasing Mach number, as apparent in Figure 6 for $\mathsf{Ma}^- = 2.5$, where the jump of u covers to a great extent the difference between asymptotic states, leaving only a flat tail downstream, whereas temperatures are very different in the shock region behind the front, with huge overshooting and with a spread that is larger than the temperature difference $T^+ - T^-$. Notice also how the shock thickness sensibly decreases for increasing Ma^- throughout Figures 2–6, as expected.

The plots above relevant to the considered reference test problem remain qualitatively similar if the input conditions are varied, and we conclude this Section by briefly discussing the main observed changes. Anisotropy of collision seems to play only some very minor role, whereas some effects show up when to collision frequencies for mechanical and chemical encounters are given different weights. So, if all elastic collision kernels $\bar{\varkappa}_{ij}$ are set equal to 0.01, the reduced collisionality strongly enhances the length of the tails, as shown in Figure 7, relevant to $\mathsf{Ma}^- = 2.5$ (thus to be compared to Figure 6), where the concentration fractions χ_i and species temperatures T_i are plotted. One can also observe here some slightly oscillating trends in the initial part of the temperature tails, as probably due to the fact that evolution is driven essentially by reactive events, which do

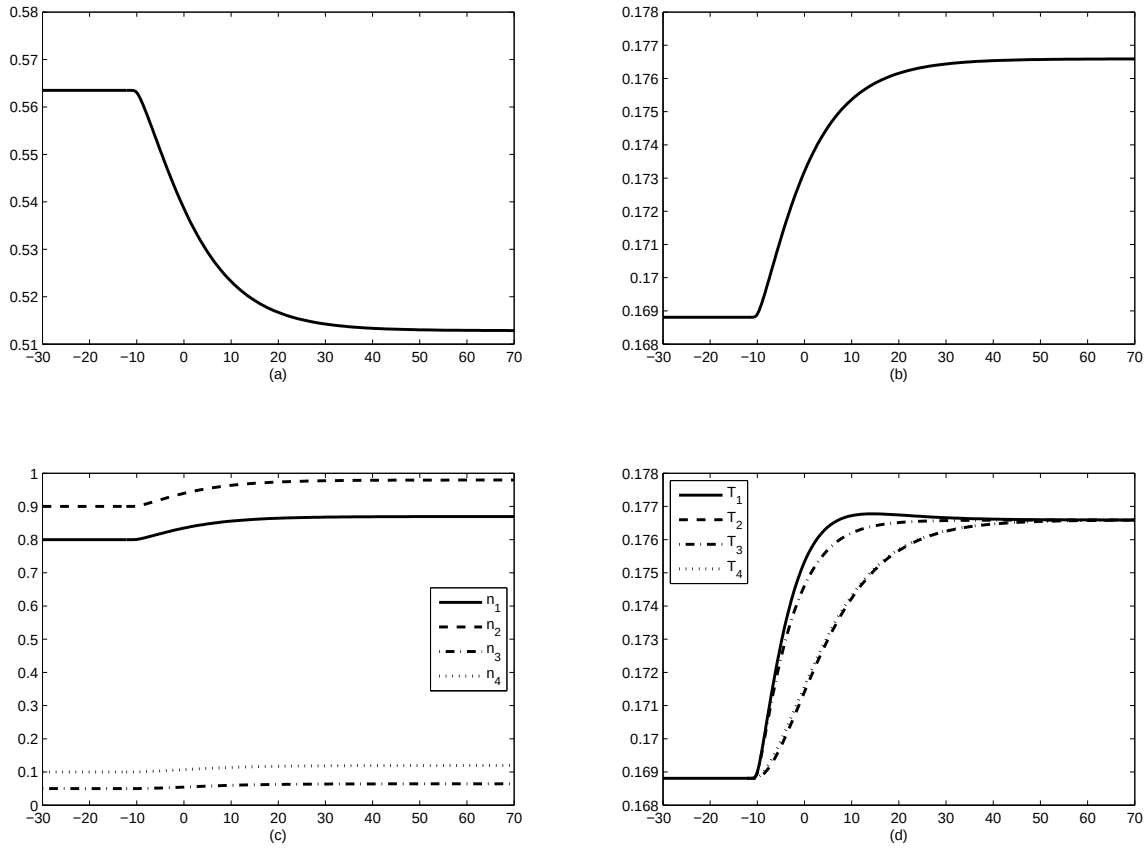

Figure 3: Mass velocity (a), gas temperature (b), species densities (c), and species temperatures (d) versus x for the reference case when $\mathsf{Ma}^- = 1.06$ (smooth solution).

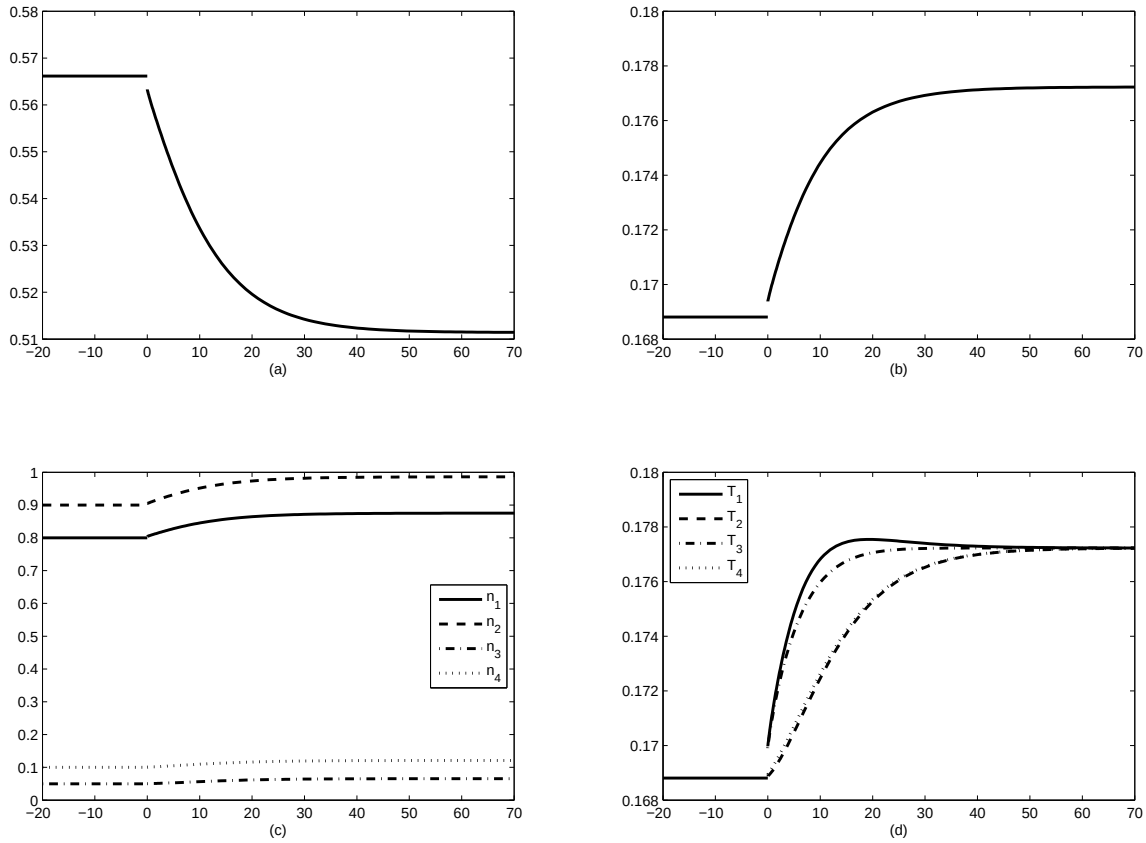

Figure 4: Mass velocity (a), gas temperature (b), species densities (c), and species temperatures (d) versus x for the reference case when $\mathsf{Ma}^- = 1.065$ (discontinuous solution).

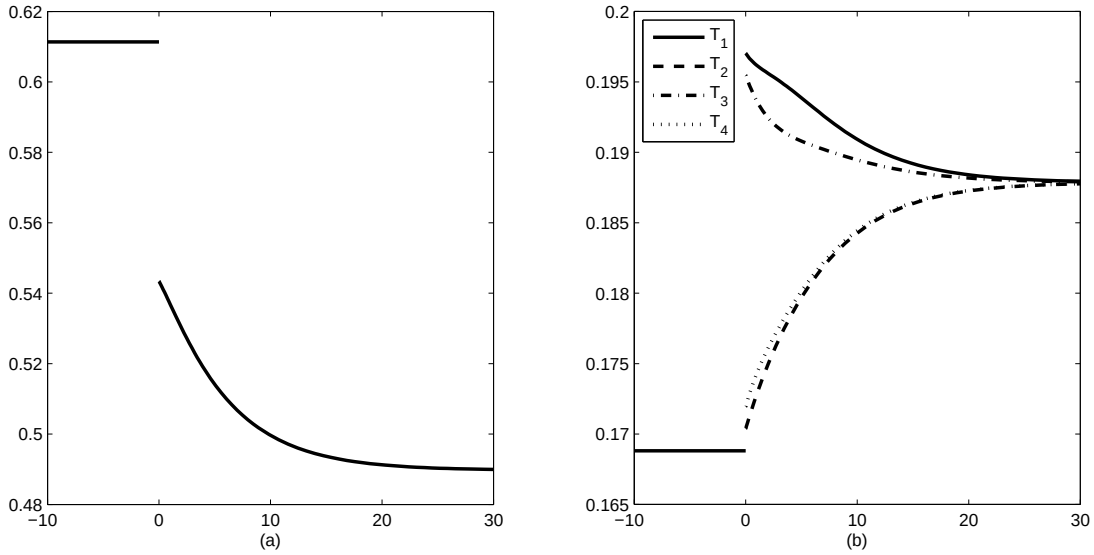

Figure 5: Mass velocity (a) and species temperatures (b) versus x for the reference case when $\mathsf{Ma}^- = 1.15$.

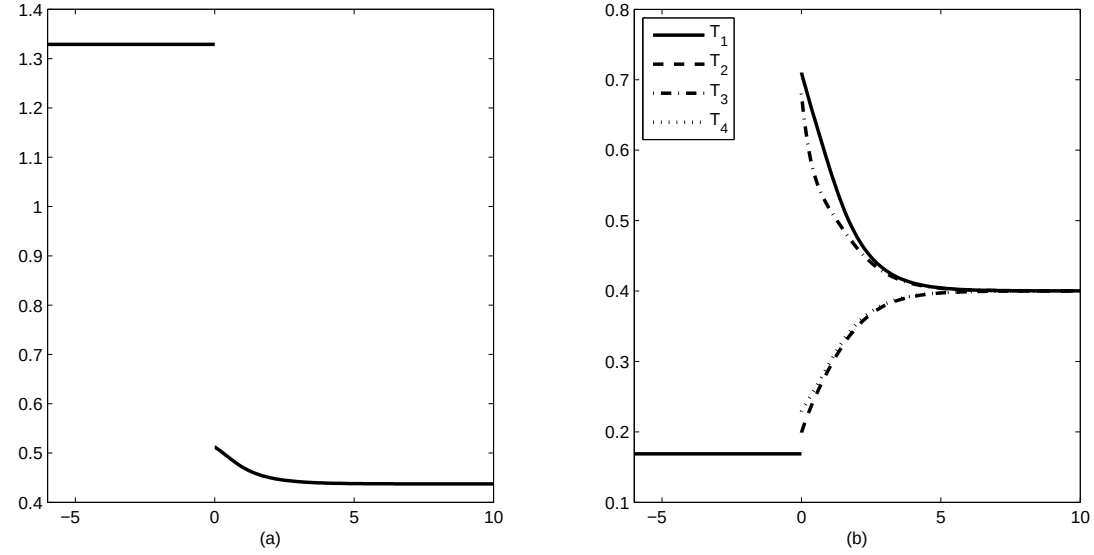

Figure 6: Mass velocity (a) and species temperatures (b) versus x for the reference case when $\mathsf{Ma}^- = 2.5$.

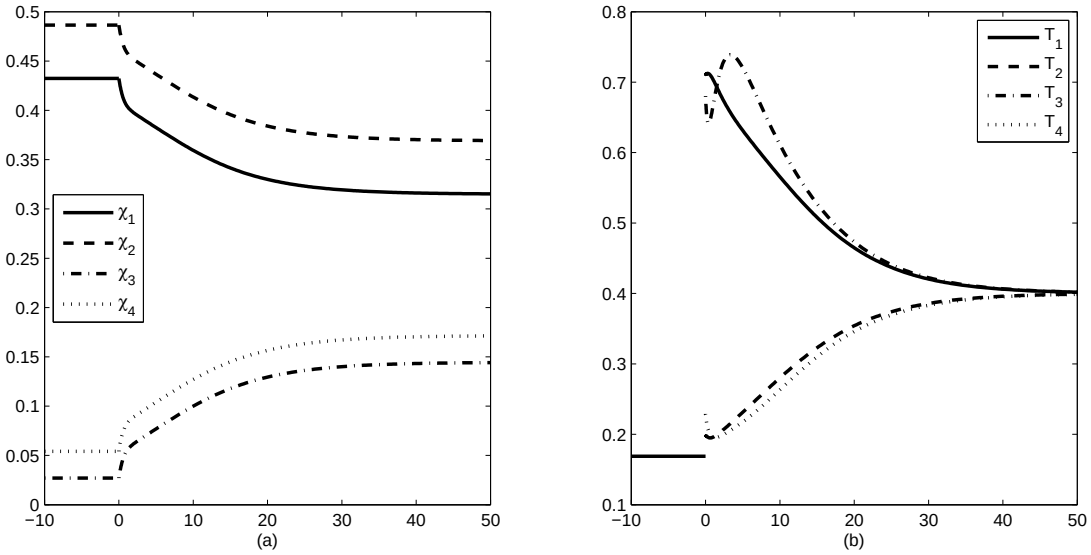

Figure 7: Concentration fractions (a) and species temperatures (b) versus x for $\mathsf{Ma}^- = 2.5$ when elastic collision kernels are reduced by a factor 10^2 with respect to the reference case.

not necessarily prescribe, by themselves, temperature equalization. The opposite effect is obviously observed if all elastic collision kernels $\bar{\varkappa}_{ij}$ are set equal to 20, as in Figure 8, relevant again to $\mathsf{Ma}^- = 2.5$, and with the same layout of Figure 7. Comparison with Figure 6 shows that convergence to downstream equilibrium (accuracy test of 10^{-4}) occurs on the scale of 2 dimensionless length units, instead of 10. Since mechanical encounters affect primarily temperature evolution, one can observe here how relaxation is faster for temperatures than for concentrations (or densities), and indeed the same accuracy test is fulfilled by temperatures already after 1 length unit.

An example of possible variation of upstream conditions is illustrated in Figure 9, left plot, where, with respect to the test case, concentrations have been changed to the more balanced distribution

$$\chi_1^- = 0.25 \qquad \chi_2^- = 0.35 \qquad \chi_3^- = 0.25 \qquad \chi_4^- = 0.15\,, \tag{51}$$

which imply a smaller critical Mach number 1.0227, and where Ma^- has been chosen as 1.1. The shown temperature profiles should be compared qualitatively to those of Figure 5. Mass ratios also play some role, and this is what the right plot of Figure 9 is about. Here, the only change with respect to the left part is that masses have been varied to

$$m_1 = 3 \qquad m_2 = 4.4 \qquad m_3 = 4.6 \qquad m_4 = 2.8 \tag{52}$$

relevant to the reaction $NO{+}CO_2 \rightleftarrows NO_2{+}CO$. Now the critical Mach number decreases further to 1.0049, so that $\mathsf{Ma}^- = 1.1$ becomes comparatively higher, which explains the stronger (relative) jump. Also, masses are now much more balanced, which implies larger exchange rates in collisions and then faster tail relaxation. Again one can notice affinity in the temperatures of species with almost equal masses: 1 with 4 and 2 with 3 here (it

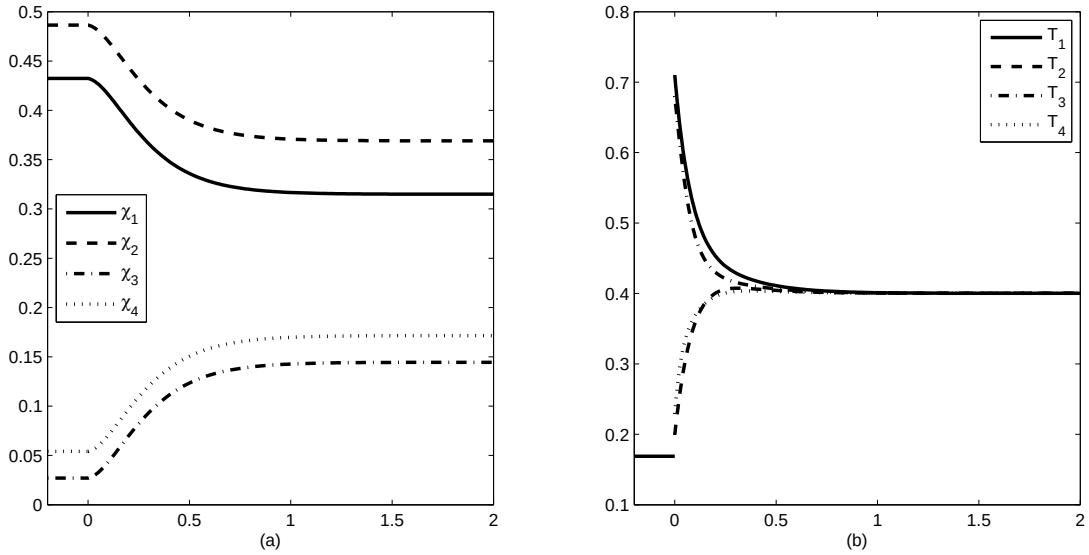

Figure 8: Concentration fractions (a) and species temperatures (b) versus x for $\mathsf{Ma}^- = 2.5$ when elastic collision kernels are increased by a factor 20 with respect to the reference case.

was 1 with 3 and 2 with 4 with masses (49)).

Acknowledgement. Work supported by the Italian National Research Project "Problemi Matematici delle Teorie Cinetiche e Applicazioni" (PRIN 2009). Fruitful discussions with T. Ruggeri and S. Simic are also gratefully acknowledged.

References

[1] V. Giovangigli, *Multicomponent Flow Modeling*, Birkhäuser, Boston, 1999.

[2] C. Cercignani, *Rarefied Gas Dynamics. From Basic Concepts to Actual Calculations*, University Press, Cambridge, 2000.

[3] E. Nagnibeda, E. Kustova, *Non–equilibrium Reacting Gas Flows*, Springer, Berlin, 2009.

[4] E. Goldman, L. Sirovich, "Equations for mixtures", *Phys. Fluids* **10** (1967), 1928–1940.

[5] E. Kustova, E. Nagnibeda, "On a correct description of a multi–temperature dissociating CO_2 flow", *Chem. Phys.* **321** (2006), 293–310.

[6] T.K. Bose, *High Temperature Gas Dynamics*, Springer, Berlin, 2003.

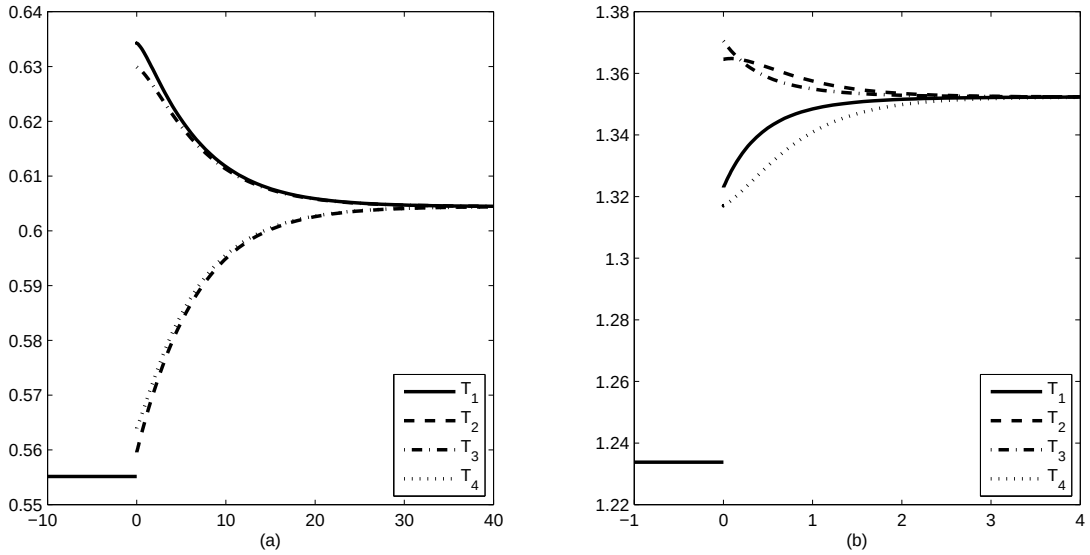

Figure 9: Species temperatures versus x for $\mathsf{Ma}^- = 1.1$ when chemical fractions upstream are varied with respect to the reference case (plot (a)). Species temperatures versus x for $\mathsf{Ma}^- = 1.1$ when additionally mass ratios are varied with respect to the reference case (plot (b)).

[7] J.D. Ramshaw, "Hydrodynamic theory of multicomponent diffusion and thermal–diffusion in multitemperature gas mixtures", *J. Non–Equilib. Thermodyn.* **18** (1993), 121–134.

[8] I. Müller, T. Ruggeri, *Rational Extended Thermodynamics*, Springer, New York, 1988.

[9] T. Ruggeri, S. Simic, "Average temperature and Maxwellian iteration in multi–temperature mixtures of fluids", *Phys. Rev. E* **80** (2009), 026317.

[10] F. Brini, "On the flame structure in multi–temperature mixture theory", *Ric. Mat.* **58** (2009), 63–76.

[11] M. Groppi, G. Spiga, "Kinetic approach to chemical reactions and inelastic transitions in a rarefied gas", *J. Math. Chem.* **26** (1999), 197–219.

[12] L. Desvillettes, R. Monaco, F. Salvarani, "A kinetic model allowing to obtain the energy law of polyatomic gases in the presence of chemical reactions", *Eur. J. Mech. B Fluids* **24** (2005), 219–236.

[13] M. Groppi, G. Spiga, F. Zus, "Euler closure of the Boltzmann equations for resonant bimolecular reactions", *Phys. Fluids* **18** (2006), 057105.

[14] M. Bisi. G. Martalò. G. Spiga, "Multi–temperature hydrodynamic limit from kinetic theory in a mixture of rarefied gases", *Acta Appl. Math.* **122** (2012), 37–51.

[15] M. Bisi, G. Martalò, G. Spiga, "Multi–temperature Euler hydrodynamics for a reacting gas from a kinetic approach to rarefied mixtures with resonant collisions", *Europhys. Lett.* **95** (2011), 55002.

[16] A. Rossani, G. Spiga, "A note on the kinetic theory of chemically reacting gases", *Physica A* **272** (1999), 563–573.

[17] T. Ruggeri, J. Lou, "Heat conduction in multi–temperature mixtures of fluids: the role of the average temperature", *Phys. Lett. A* **373** (2009), 3052–3055.

[18] L. Landau, "On the vibrations of the electronic plasma", *J. Phys. U.S.S.R.* **10** (1946), in *Collected Papers of L.D. Landau*, edited by D. ter Haar, pp. 445–460, Pergamon Press, Oxford, 1965.

[19] M. Groppi, A. Rossani, G. Spiga, "Fluid–dynamic model equations for a gas with slow reversible bimolecular reactions", *Comm. Math. Sci.* **7** (2009), 143–163.

[20] M. Groppi, G. Spiga, S. Takata, "The steady shock problem in reactive gas mixtures", *Bullet. Inst. Math. Acad. Sinica (New Series)* **2** (2007), 935–956.

[21] G. Boillat, T. Ruggeri, "On the shock structure problem for hyperbolic system of balance laws and convex entropy", *Continuum Mech. Thermodyn.* **10** (1998), 285–292.

[22] W.G. Vincenti, C.H. Kruger, *Introduction to Physical Gas Dynamics*, Wiley, New York, 1965.

[23] M. Groppi, K. Aoki, G. Spiga, V. Tritsch, "Shock structure analysis in chemically reacting gas mixtures by a relaxation-time kinetic model", *Phys. Fluids* **20** (2008), 117103.

[24] M. Groppi, S. Rjasanow, G. Spiga, "A kinetic relaxation approach to fast reactive mixtures: shock wave structure", *J. Stat. Mech.* **09** (2009), P10010.